Int J Adv Manuf Technol (2017) 90:2813–2826
DOI 10.1007/s00170-016-9530-3

ORIGINAL ARTICLE

Influence of feedstock properties on the injection molding of aluminum nitride

Kunal H. Kate[1] · **Ravi K. Enneti**[2] · **Sundar V. Atre**[1]

Received: 4 July 2016 / Accepted: 25 September 2016 / Published online: 22 October 2016

Abstract Powder injection-molding (PIM) simulations are useful to identify appropriate combinations of material, process, and geometry variables required for successful manufacturing outcomes. PIM simulations can identify optimized processing parameters without the requirement of expensive trials when changes are made to feedstock composition or geometry design. However, PIM simulations require physical, thermal, and rheological feedstock properties as input data that require additional time, expertise, and expense. Whereas injection-molding simulation platforms typically offer over 5000 listings of property datasets for polymers, there are presently fewer than 5 such listings for ceramics and metals. The present work compares experimentally measured physical, thermal, and rheological properties for an aluminum nitride (AlN) feedstock to estimated values based on known filler properties and semi-empirical models. Injection-molding experimental studies carried out on a simple test geometry showed reasonable correspondence to PIM simulations using the two datasets. Further, mold-filling simulations were performed on complex heat-sink substrate geometries to compare the output of PIM simulations using experimentally measured and estimated feedstock property datasets. The present study indicates the merit of using estimated feedstock properties as input parameters in mold-filling simulations that could be extended for a variety of material systems and geometries early in the PIM design stage.

✉ Sundar V. Atre
sundar.atre@louisville.edu

[1] University of Louisville, 2210, S Brook Street, Shumaker Research Building, 214, Louisville, KY 40208, USA

[2] Global Tungsten and Powders Corporation, 1 Hawes Ln, Towanda, PA 18848, USA

Keywords Powder injection molding · Simulations · Material properties · PIM · Estimation · Aluminum nitride

1 Introduction

Powder injection molding (PIM) is a net-shaping process used to manufacture parts with complex shapes at high production volumes with metals or ceramics. Utilizing computer-aided engineering (CAE) tools early in the design stage can enable further growth in the $2 billion industry [1]. CAE tools are useful to evaluate appropriate process settings, mold and part geometry design, and feedstock properties necessary to manufacture superior quality parts [2–6]. Common CAE tools include Autodesk Moldflow, Sigmasoft, PIMsolver, and Modelx3D. CAE design tools depend on the availability of powder-polymer mixture (feedstock) property data such as density, specific heat, viscosity, thermal conductivity, viscosity, and specific volume. In order to support the design engineer to perform injection simulations of plastics, the CAE design tools typically list complete property datasets for around 5000 polymers. However, fewer than five such property datasets are available for metal and ceramic injection-molding feedstocks in these CAE tools. This situation presents a significant barrier to the use of metal and ceramics in injection-molding process and product design.

American Society for Testing and Materials (ASTM) standards exist for measuring material properties that are required to perform PIM simulations. However, changes in feedstock composition may be needed to address manufacturing defects. Subsequently, new measurements of feedstock properties would be required to conduct additional simulations, significantly adding to costs and delays in proceeding from design to production. To address this issue, a recent paper from our research group evaluated several models to estimate feedstock

properties for any powder-polymer composition [4]. That study identified models that appear to best predict thermal, physical, and rheological properties based on existing literature data on filled polymers.

In the present study, aluminum nitride (AlN) feedstock properties estimated using this procedure were compared with experimental measurements. The aim of the present paper is to understand the influence of feedstock properties from experiments and estimations on predictions derived from mold-filling simulations.

The current work focuses on three major issues. Firstly, AlN feedstock was prepared and its properties such as density, specific heat, thermal conductivity, viscosity, and pressure-volume-temperature parameters were experimentally measured. Semi-empirical equations were simultaneously used to also estimate these properties. Secondly, injection-molding experiments were performed using the AlN feedstock on a simple tensile-bar geometry to test the results of mold-filling simulations. Thirdly, the experimental and estimated feedstock property datasets were used to conduct injection-molding simulations on complex heat-sink geometries, a common application for AlN, and consequently identify the feedstock properties that had the most influence on the results of mold-filling predictions.

2 Experimental and simulation methods

AlN feedstock used in the study was prepared using a twin-screw extruder with length-to-diameter (L/D) ratio of 40. The AlN feedstock consisted of a powder-polymer mixture with 80.5 wt.% AlN powders (median particle size, 1.1 μm) and 19.5 wt.% binder. The binder comprised paraffin wax, a low-density polyethylene, a modified polypropylene, and stearic acid. Details of the binder composition and feedstock compounding are provided elsewhere [7, 8]. Material property measurements were made for the AlN feedstock and the unfilled wax-polymer binder for density, thermal conductivity, specific heat, viscosity, and PvT parameters at Datapoint Labs (Ithaca, NY).

The solid density was measured according to Archimedes principle and ASTM D792 standard. The melt density measurement was done using a capillary rheometer in accordance with ASTM D3835. The specific heat was measured with ASTM E1269 using differential scanning calorimetry (DSC). The thermal conductivity was measured based on ASTM D5930 using a transient line-source technique. The viscosity was measured using ASTM D3835 on a capillary rheometer. The pressure-volume-temperature values (PvT) were measured according to ASTM D792 using a high-pressure dilatometer.

Mold-filling simulations were performed using Autodesk Moldflow software. The software is capable of simulating results in three dimensions (3D) and uses a finite element method (FEM) for calculating velocity, temperature, and pressure profiles in defined geometry. To analyze FEM results, the defined geometry is dived into smaller elements that are joined together by the means of a mesh. Results are calculated for each element in the mesh. The typical mesh types are mid-plane, dual-domain, and 3D in Autodesk Moldflow. Mold-filling simulations were performed using estimated and experimental feedstock properties of AlN to understand the influence of scatter in feedstock property estimates on mold-filling behavior.

The testing studies to estimate the accuracy of simulations were carried out using AlN feedstock on a tensile-bar geometry (Fig. 1). The AlN feedstock was injection molded into a tensile geometry using an Arburg 221M injection-molding machine. An injection gate with a size of 6.5 mm was used to inject the AlN feedstock into the mold cavity. Injection-molding experiments were performed at a melt temperature of 444 K and injection pressure of 14 MPa by keeping the flow rate constant at 33 cm^3/s to obtain parts with complete mold fill. The applicability of simulations in practical applications was studied on two types of heat-sink substrate geometries shown in Fig. 2. Solidworks software was used to design these heat-sink substrate geometries. A heat-sink substrate without fins **(**Fig. 2a**)** and a heat-sink substrate with fins **(**Fig. 2b**)** were designed to understand the influence of geometry design on injection-molding output parameters and feedstock properties. The two heat-sink substrate geometries were imported into the Autodesk Moldflow software and meshed using a "3D" mesh type (150,000 mesh elements) to conduct mold-filling simulations. A 3D mesh type was selected as it provides most accurate 3D representation of results in thick or thin solid regions in the part when compared with mid-plane and dual-domain mesh types.

3 Results and discussion

3.1 Feedstock property estimation requirements

Aluminum nitride feedstock properties were estimated for density, thermal conductivity, specific heat, viscosity, and PVT parameters. Select semi-empirical equations were used that estimate feedstock properties as a function of composition, AlN filler, and binder property values. Several literature reports were studied to gather AlN filler property data for density, specific heat, and thermal conductivity. Filler properties collected from literature were reported for 300 K **(**Table 1**)**. Twenty-two values of density for AlN were gathered from the literature [1–13, 29, 30]. It can be observed from Table 1 that the AlN filler density was 3250 ± 50 kg/m^3. The reciprocal of the density values were also used to estimate the

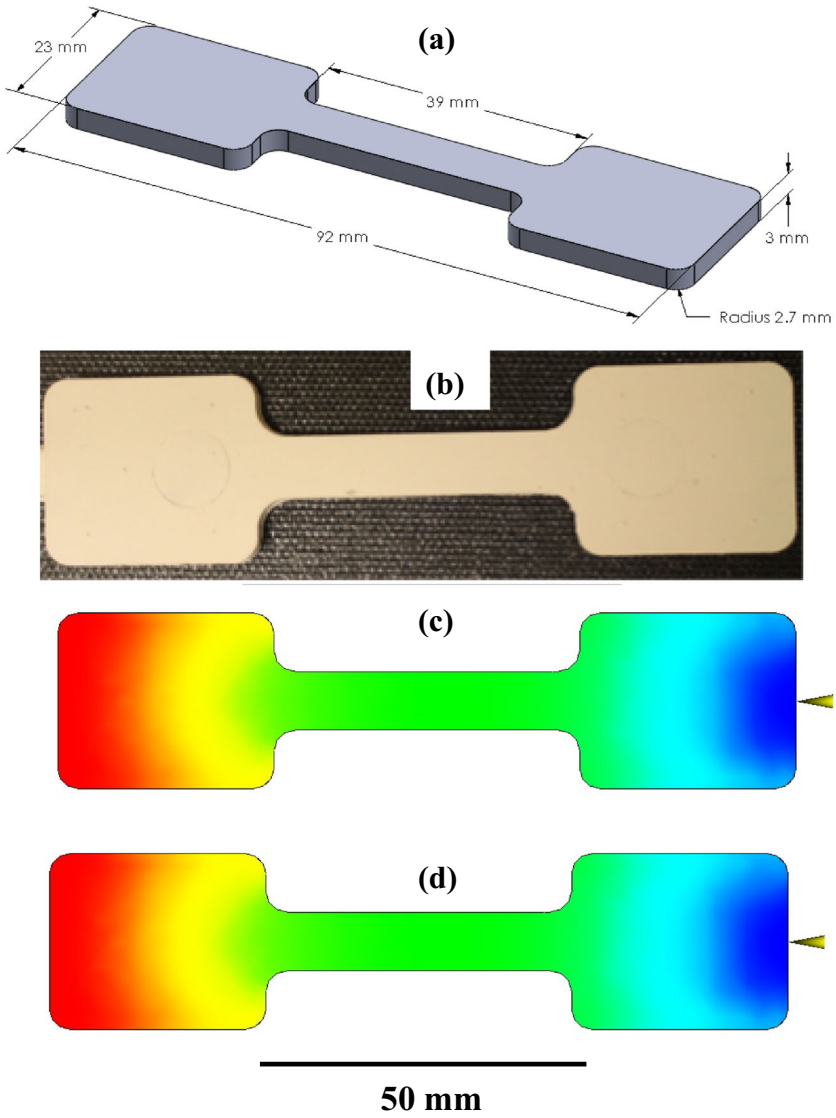

Fig. 1 Injection molding testing and simulations on **a)** tensile bar geometry, **b)** 100 % filled AlN tensile-bar geometry with experiments, **c)** 100 % filled AlN tensile bar geometry using experimental dataset (Table 9), and **d)** 100 % filled AlN tensile bar geometry using dataset 1 (Table 9)

filler-specific volume for AlN. Six data points of specific heat for AlN were gathered from literature [20, 30–32]. It can be observed from Table 1 that AlN filler-specific heat was 800 ± 30 J/kg K. Eighteen values of thermal conductivity for AlN were gathered from literature [11, 13, 17–19, 21, 22, 24, 30, 33]. It can be observed from Table 1 that AlN filler thermal conductivity was 230 ± 70 W/m K.

Experimentally measured feedstock properties were compared with estimations based on filler property values for each physical, thermal, and rheological property using models described in the rest of the sections.

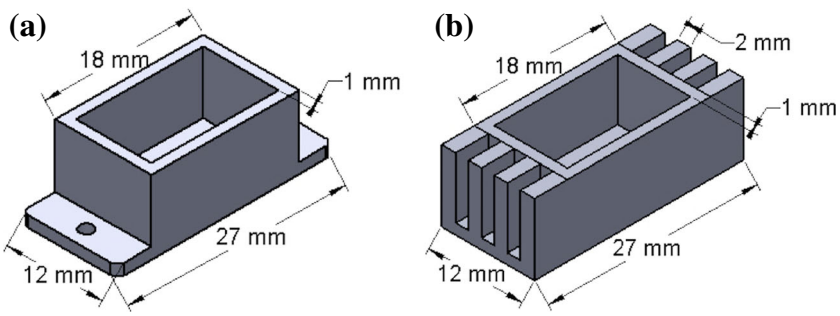

Fig. 2 Mold geometry used for injection molding simulation **(a)** heat-sink substrate without fins and **(b)** heat-sink substrate with fins

Table 1 Literature filler properties of AlN fillers at 300 K

Filler	Solid density[a] (ρ_p, kg/m^3)	Specific heat[b] (C_{p_p}, J/kg K)	Thermal conductivity[c] (λ_p, W/m K)	Reference no.
AlN	3250 ± 50	800 ± 30	230 ± 70	[6, 9–28]

* ρ_p has 22 data points

+ C_{p_p} has 6 data points

++ λ_p has 18 data points

3.1.1 Density

Density measurements are required in injection-molding simulations to predict part weight and variations in density that occur inside the mold geometry.

Density measurements Table 2 summarizes the experimental density of AlN feedstock used in this study. The solid density of AlN feedstock was experimentally measured to be 2150 kg/m^3, and melt density was experimentally measured as 1940 kg/m^3. The solid and melt densities of the wax-polymer binder were measured to be 880 and 730 kg/m^3, respectively [7, 8].

Density estimates An inverse rule of mixtures (Eq. 1) was used to estimate solid and melt density of AlN feedstock. This equation has been previously evaluated to be suitable for predicting powder-polymer density at higher weight fractions of fillers [29]. Equation 1 provides a coefficient of determination (R^2) of 0.97 when fitted to literature data on measured powder-polymer densities (50–70 wt.%).

$$\frac{1}{\rho_c} = \frac{X_b}{\rho_{b\ exp}} + \frac{X_p}{\rho_p} \tag{1}$$

X_p is weight fraction of AlN filler (0.805), X_b is weight fraction of wax-polymer binder (1–X_p) and ρ_c, $\rho_{b\ exp}$, and ρ_p represent density of composite, binder, and filler, respectively.

The AlN filler density (ρ_p) values were obtained from literature as listed in Table 1. The binder density ($\rho_{b\ exp}$) value was used from the experimental value in Table 2. The solid and melt density of AlN feedstock was estimated for 22 data points of AlN filler density (Table 1). In Table 2, numbers in italics represent experimentally measured values of ρ_c and $\rho_{b\ exp}$. The estimated values of average solid and melt density ($\rho_{c\ avg}$) were 2130 and 1940 kg/m^3. The estimated minimum values for solid and melt density ($\rho_{c\ min}$) were 2050 and 1880 kg/m^3. The estimated maximum values for solid and melt density ($\rho_{c\ max}$) were 2150 and 1960 kg/m^3. The estimated average ($\rho_{c\ avg}$), maximum ($\rho_{c\ min}$), and minimum ($\rho_{c\ max}$) density values from Table 2 were used to create the dataset necessary for performing mold-filling simulations.

The composition of the AlN feedstock is experimentally determined by weighing the components prior to mixing. Therefore it is useful to report these values on a on a weight-fraction basis. However, several material properties such as viscosity and thermal conductivity require volume fraction as basis [29]. To calculate volume fraction the feedstock solid and binder density in Table 2 were used in conjunction with Eqs. 2 and 3.

$$\phi_p = \frac{X_p \Big/ \rho_p}{X_p \Big/ \rho_p + X_b \Big/ \rho_{b\ exp}} \tag{2}$$

$$\phi_b = \frac{X_b \Big/ \rho_b}{X_p \Big/ \rho_p + X_b \Big/ \rho_{b\ exp}} \tag{3}$$

ϕ_p and ϕ_b are binder and powder volume fractions. ϕ_p was calculated as 0.52 and ϕ_b was calculated as 0.48.

3.1.2 Specific heat

Specific heat measurements are required in injection-molding simulations to model the heat transfer during mold filling, packing, and cooling stages.

Specific heat measurements Specific heat measurements were made for the AlN feedstock and the wax-polymer binder for a temperature range between 280 and 450 K. The data is represented in Table 3. It was observed that the specific heat of the wax-polymer binder initially increased up to the transition temperature of the binder (320 K) and showed a decrease in specific heat with further increase in temperature. Specific heat of wax-polymer binder $\left(C_{p_{b\ exp}}\right)$ ranged between 2080 and 4640 J/kg K and AlN feedstock $\left(C_{p_{c\ exp}}\right)$ ranged between 920 and 1210 J/kg K [7, 8].

Table 2 Density of AlN feedstock and wax-polymer binder at 300 K

Density (^{3}/kg)	$\rho_{b\ exp}$[a]	$\rho_{c\ exp}$[a]	$\rho_{c\ est}$[b]
Solid	*880*	*2150*	2130 ± 20
Melt	*730*	*1940*	1940 ± 20

[a] Measured experimentally

[b] Estimated using Eq. 1 for 22 data points of ρ_p from Table 1

Table 3 Specific heat of AlN feedstock and wax-polymer binder for temperature between 283 and 423 K

Specific heat C_p (J/kg K)	Temperature (K)				
	283	298	331	374	423
$C_{p_b exp}$ [a]	2080	3360	4640	3490	2530
$C_{p_c exp}$ [a]	920	1110	1090	1130	1210
$C_{p_c est}$ [b]	1050 ± 35	1240 ± 35	1570 ± 35	1850 ± 35	1150 ± 35

[a] Measured experimentally

[b] Estimated using Eq. 4 for 6 data points of C_{p_p} from Table 1

Specific heat estimates Several mathematical models have been published in literature that can estimate specific heat of a powder-polymer mixture [29]. In the present study, a modified rule-of-mixtures model (Eq. 4) was used to estimate specific heat. Equation 4 provides R^2 values ranging from 0.92 to 0.97 when fitted to literature data on measured specific heats of five 47–75 wt.% filled-polymer systems [29]. The specific heat of AlN feedstock was estimated using Eq. 4 for 80.5 wt.% AlN feedstock.

$$C_{p_c} = \left(C_{p_{b\ exp}} X_b + C_{p_p} X_p\right) \times \left(1 + A \times X_b X_p\right) \quad (4)$$

X_p is weight fraction of AlN feedstock (0.805), and X_b is weight fraction of wax-polymer binder. C_{pc}, $C_{p_{b\ exp}}$, and C_{p_p} represent specific heats of composite, binder, and filler, respectively. A is a fitting constant for spherical powders with a value of 0.2.

To make estimates, the specific heat of AlN feedstock for a temperature range of 280 to 430 K and the polymer binder-specific heat ($C_{p_{b\ exp}}$) for corresponding temperatures was taken from Table 1 [7, 8]. There is a lack of literature data for specific heat values of AlN over the temperature range of interest. It was therefore assumed that specific heat of AlN filler remained constant between 280 and 430 K.

The values for AlN filler-specific heats $\left(C_{p_p}\right)$ were obtained from literature and are reported in Table 1. The binder-specific heat $\left(C_{p_b exp}\right)$ value for temperatures between 283 and 423 K were experimentally measured and reported in Table 3. The specific heat of AlN feedstock was estimated for 6 data points of AlN filler-specific heat (Table 1). The estimated average ($C_{pc\ avg}$), maximum ($C_{pc\ max}$), and minimum ($C_{pc\ min}$) specific heat values from Table 3 were used to create a data set necessary for performing mold-filling simulations.

3.1.3 Thermal conductivity

Thermal conductivity measurements are required in injection-molding simulations to model the heat transfer during mold filling, packing, and cooling stages.

Thermal conductivity measurements Thermal conductivity measurements for AlN feedstock and the wax-polymer binder were made for a temperature range between 316 and 436 K. Representative experimental measurements are shown as bold values in Table 4. It was observed that the thermal conductivity of the wax-polymer binder decreased with an increase in temperature. The thermal conductivity measurements of AlN feedstock followed a similar trend. The thermal conductivity of the wax-polymer binder ($\lambda_{b\ exp}$) ranged between 0.162 and 0.195 W/m K. The AlN feedstock ($\lambda_{b\ exp}$) ranged between 2.06 and 4.26 W/m K [7, 8].

Thermal conductivity estimates The Maxwell model, Bruggeman model, and a modified Lichtenecker model have

Table 4 Thermal conductivity of AlN feedstock and wax-polymer binder for temperature between 316 and 436 K

Thermal conductivity (W/m K)	Temperature (K)				
	316	356	377	397	436
$\lambda_{b\ exp}$ [a]	0.195	0.182	0.176	0.171	0.162
$\lambda_{c\ exp}$ [a]	4.26	2.23	2.66	2.06	2.50
$\lambda_{c\ est}$ [b]	1.82 ± 0.01	1.71 ± 0.01	1.67 ± 0.06	1.62 ± 0.08	1.55 ± 0.10

[a] Measured experimentally

[b] Estimated using Eq. 5 for 6 data points of λ_p from Table 1

been previously used to estimate thermal conductivity [29]. In the present study, the Bruggeman model (Eq. 5) was used to estimate thermal conductivity of 52 vol.% AlN feedstock [29].

$$1-\phi_p = \left(\frac{\lambda_p-\lambda_c}{\lambda_p-\lambda_{b\,exp}}\right)\left(\frac{\lambda_b}{\lambda_c}\right)^{1/3} \quad (5)$$

ϕ_p is the volume fraction of AlN feedstock (0.52). λ_c, λ_{bexp}, and λ_p represent thermal conductivities of the composite, binder, and filler, respectively.

In order to estimate the thermal conductivity of AlN feedstock for a temperature range of 310 to 440 K, the binder thermal conductivity ($\lambda_{b\,exp}$) were taken from Table 4 [7, 8]. The values for AlN filler thermal conductivities (λ_p) were obtained from literature and taken from Table 1. There is limited availability of literature data for thermal conductivity of AlN filler for a range of temperature. It was assumed that thermal conductivity of AlN filler remains constant between 310 and 440 K. The thermal conductivity of AlN feedstock was estimated for 18 data points of AlN filler thermal conductivity (Table 1). Table 4 shows the estimated thermal conductivity as a function of experimental thermal conductivity for a range of temperatures of AlN feedstock. The estimated average ($\lambda_{c\,avg}$), maximum ($\lambda_{c\,max}$), and minimum ($\lambda_{c\,min}$) thermal conductivity values from Table 4 were used to create datasets necessary for performing mold-filling simulations.

3.1.4 Viscosity

Viscosity measurements are required in injection-molding simulations to understand the flow characteristics of the feedstock melt. It is one of most important properties required to predict output parameters such as injection pressure and clamp force.

Viscosity measurements Viscosity measurements for the AlN feedstock and the wax-polymer binder were performed for temperatures of 415, 420, 425, and 430 K and shear rates from 10 to 10^4 s^{-1} are represented in Fig. 3. It was observed that the viscosity of the wax-polymer binder and AlN feedstock decreased with an increase in shear rate and temperature (Fig. 3). A representative version of AlN feedstock viscosity data from Fig. 3 is shown in Table 5.

Viscosity estimates The Chong model, Eiler model, Mooney model, and Krieger Dougherty model have been previously used to estimate viscosity [29]. In the present study, a simplified Krieger Dougherty model (Eq. 6) was used to estimate viscosity. Equation 6 provides R^2 values ranging from 0.94 to 0.99 when fitted to literature data on measured viscosity of three 50–60 vol.% filled-polymer systems.

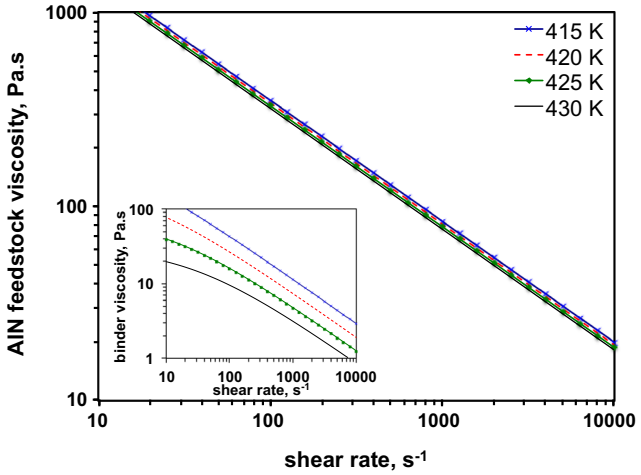

Fig. 3 Experimentally measured viscosity of AlN feedstock and wax-polymer binder (*inset*) for a shear rate range of 10 to 10^4 s^{-1} and a temperature range between 415 and 430 K

$$\eta_c = \frac{\eta_{b\,exp}}{\left(1-\frac{\phi_p}{\phi_{max}}\right)^2} \quad (6)$$

η_{bexp} is the viscosity of binder, η_c is the viscosity of feedstock, ϕ_p is volume fraction of feedstock, and ϕ_{max} is the volume fraction of critically loaded feedstock.

Viscosity of the AlN feedstock was estimated for 40 different shear rates in ranges between 10 and 10^4 s^{-1} and for temperatures 415, 420, 425, and 430 K using Eq. 6 and polymer binder viscosity ($\eta_{b\,exp}$) values from Fig. 1. The volume fraction of AlN feedstock (ϕ_p) was calculated to be 0.52 using Eq. 2. Viscosity was estimated for ϕ_{max} of 0.6, 0.64, and 0.68 critical filler content.

To perform mold-filling simulations, the viscosity of had to be represented in terms of fitted constants. A cross-WLF equation (Eq. 7) was used to extract fitted constants for ϕ_{max} of 0.6, 0.64, and 0.68.

$$\eta = \frac{\eta_0}{1+\left(\frac{\eta_0\gamma}{\tau^*}\right)^{1-n}} \quad (7)$$

η is the melt viscosity (Pa s), η_0 is the zero shear viscosity, γ is the shear rate (1/s), τ^* is the critical stress level at the transition to shear thinning and is determined by curve fitting, and n is the power-law index in the high shear rate regime. Power-law index, n is also determined by curve fitting.

The temperature dependence of viscosity of any powder-polymer mixture can be calculated using Eq. 8.

$$\eta_0 = D_1 \exp\left(-\frac{A_1\left(T-T^*\right)}{A_2+\left(T-T^*\right)}\right) \quad (8)$$

T is the temperature (K). T^*, D_1, and A_1 are curve-fitted coefficients. A_2 is the WLF constant and is assumed to be 51.6 K.

Table 5 Viscosity of AlN feedstock as a function of shear rate between 10^1 and 10^4 s^{-1} and a temperature range of 415–430 K

Shear rate (s^{-1})	Viscosity η_c, (Pa s: T = 415 K)				Viscosity η_c (Pa s: T = 425 K)				Viscosity η_c (Pa s: T = 430 K)			
	$\eta_{c\ exp}$ [a]	$\eta_{c\ min}$ [b] (ϕ_{max} = 0.68)	$\eta_{c\ avg}$ [b] (ϕ_{max} = 0.64)	$\eta_{c\ max}$ [b] (ϕ_{max} = 0.60)	$\eta_{c\ exp}$ [a]	$\eta_{c\ min}$ [b] (ϕ_{max} = 0.68)	$\eta_{c\ avg}$ [b] (ϕ_{max} = 0.64)	$\eta_{c\ max}$ [b] (ϕ_{max} = 0.60)	$\eta_{c\ exp}$ [a]	$\eta_{c\ min}$ [b] (ϕ_{max} = 0.68)	$\eta_{c\ avg}$ [b] (ϕ_{max} = 0.64)	$\eta_{c\ max}$ [b] (ϕ_{max} = 0.60
10^1	1470	2930	4830	10,500	1380	810	1330	2890	1340	400	660	1430
10^2	350	890	1460	3170	330	330	540	1170	320	190	890	690
10^3	80	240	390	840	80	100	160	350	80	60	100	230
10^4	20	60	100	210	20	30	40	90	20	20	30	60

[a] Measured experimentally
[b] Estimated using Eq. 6

Table 6 presents the cross-WLF constants extracted from experimental viscosity data of wax-polymer binder ($\eta_{b\ exp}$) and from estimated viscosity data using Eqs. 7 and 8. The values of these constants were obtained by curve fitting the estimated viscosity for ϕ_{max} of 0.6, 0.64, and 0.68 and are represented as η_{cmax}, $\eta_{c\ avg}$, and η_{cmin}, respectively, in Table 6.

3.1.5 Specific volume

Specific volume measurements are required in injection-molding simulations to calculate the shrinkage that occurs when a feedstock is cooled from melt temperature to ambient temperature.

Specific volume measurements Mold-filling simulations require specific volume data of feedstock's typically for temperature range between 298 and 453 K and pressure range between 0 and 200 MPa. For these temperatures, the experimentally measured values of specific volume of AlN feedstock and a wax-based polymer binder are shown in Fig. 4a, b respectively shows for various temperatures and at 100 MPa pressure, as an example. Similar measurements were performed for a range of pressures of relevance to injection molding. A representative version of AlN feedstock viscosity data from Fig. 4 is shown in Table 7.

Specific volume estimates A rule-of-mixtures (Eq. 9) was used to estimate specific volume of AlN feedstock. It has been found to be suitable for predicting the powder-polymer-specific volume at higher weight fractions of fillers [29]. Equation 9 provided an R^2 value of 0.99 when fitted to literature data on measured specific volume for two 20–80 wt.% filled material systems [29]. To estimate specific volume for a range of temperature and pressure of AlN feedstock a simple empirical equation **(**Eq. 9**)** was used.

$$\upsilon_c = X_p \upsilon_p + \upsilon_{b\ exp}\left(1 - X_p\right) \tag{9}$$

To calculate the specific volume of AlN filler, the reciprocal of density of AlN filler was used **(**Table 1**)**. The density of AlN was gathered at 300 K from 22 values in the literature. Table 7 shows estimated and experimental specific volumes of AlN feedstock as a function of temperatures and pressure. In order to estimate specific volume of AlN feedstock for a range of temperatures and pressures, it was assumed that specific volume of AlN filler does not change with temperature and pressure.

The specific volume for AlN feedstocks was estimated for average, maximum, and minimum values of AlN filler specific volume. The specific volume of AlN filler was calculated from the inverse of AlN filler density values from Table 1. Additionally, to perform mold-filling simulations in Moldflow Insight software, specific volume of AlN feedstock needs to

Table 6 Cross-WLF constants for AlN feedstock

Cross-WLF constants	$\eta_{c\ exp}$ [a]	$\eta_{c\ min}$ [b] (ϕ_{max} = 0.68)	$\eta_{c\ avg}$ [b] (ϕ_{max} = 0.64)	$\eta_{c\ max}$ [b] (ϕ_{max} = 0.60
n	0.38	0.40	0.40	0.40
τ^* (Pa)	180	58,300	26,860	16,300
D_1 (Pa s)	8.78×10^{10}	2.23×10^{15}	2.23×10^{15}	2.23×10^{15}
D_2 (K)	263	361.95	360.93	360.17
A_1 (K/Pa)	14.24	48.49	49.55	50.19
A_2 (K)	51.60	51.60	51.60	51.60

[a] Calculated from Eqs. 7 and 8 and experimental (η_c) values from Table 5

[b] Calculated from Eqs. 7 and 8 and estimated (η_c) values from Table 5

be represented in terms of fitted constants. A Dual-domain Tait equation (Eq. 10) was used to extract these fitted constants for average, maximum, and minimum AlN feedstocks specific volumes. Table 8 presents the Dual-domain Tait constants extracted for estimated average $\nu_{c\ avg}$, estimated maximum $\nu_{c\ max}$, and estimated minimum $\nu_{c\ min}$ specifc volume. These values were obtained using Eq. 10

$$\upsilon(T,c) = \upsilon_o(T)\left(1 - C\ln\left(1 + \frac{p}{B(T)}\right) + \upsilon_t(T,p)\right) \quad (10)$$

$\upsilon(T,c)$ is the specific volume at a given temperature and pressure, υ_o is the specific volume at zero gauge pressure, T is temperature in K, p is pressure in pascals, and C is a constant assumed as 0.0894. The parameter B accounts for the pressure sensitivity of the material and is separately defined for the solid and melt regions. For the upper bound when $T > T_t$ (volumetric transition temperature), B is given by Eq. 11.

$$\upsilon_o = b_{1m} + b_{2m}(T - b_5) \quad (11)$$
$$B(T) = b_{3m}e^{[-b_{4m}(T-b_5)]}$$
$$\upsilon_t(T,p) = 0$$

b_{1m}, b_{2m}, b_{3m}, b_{4m}, and b_5 are curve-fitted coefficients. For the lower bound, when $T < T_t$, the parameter, B, is given by Eq. 12.

$$\upsilon_o = b_{1s} + b_{2s}(T - b_5) \quad (12)$$
$$B(T) = b_{2s}e^{[-b_{4s}(T-b_5)]}$$
$$\upsilon_t(T,p) = b_7e^{[b_8(T-b_5)-(b_9p)]}$$

b_{1s}, b_{2s}, b_{3s}, b_{4s}, b_5, b_7, b_8, and b_9 are curve-fitted coefficients. The dependence of the volumetric transition temperature T_t on pressure can be given by Eq. 13

$$T_t(p) = b_5 + b_6(p) \quad (13)$$

Dual-domain Tait constants from Table 8 were further used to create a dataset necessary for performing mold-filling simulations.

3.2 Simulation testing

The approach presented in current study uses material property estimates to perform injection-molding simulations. Testing studies were carried out to understand the accuracy of simulations. The testing studies were carried out using AlN

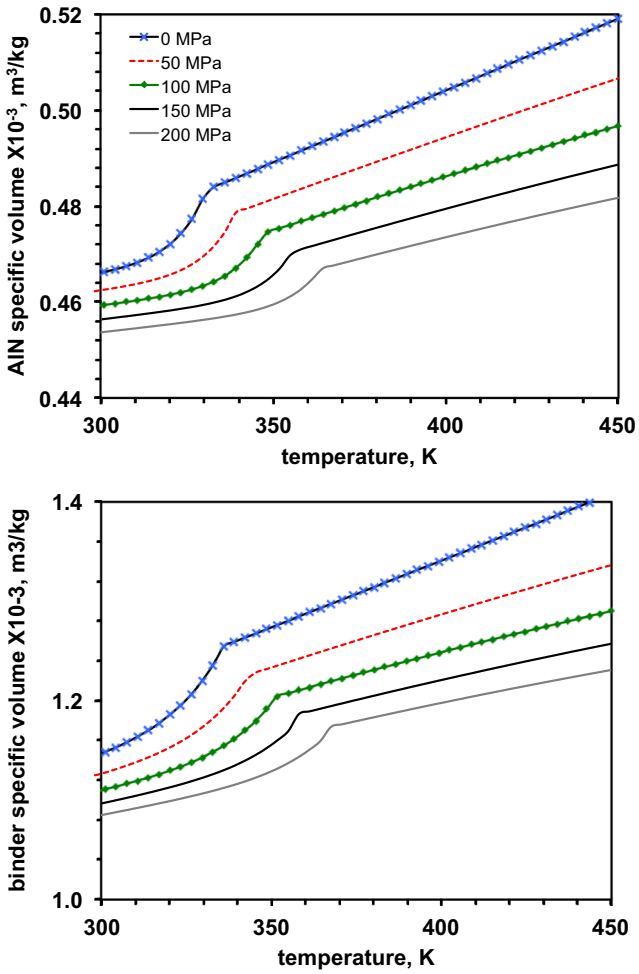

Fig. 4 Experimentally measured specific volume of **a)** AlN feedstock and **b)** wax-based polymer-binder for a temperature range of 300 to 450 K and pressures between 0 and 200 MPa

Table 7 Specific volume of AlN feedstock as a function of pressures between 0 and 200 MPa and temperature range of 300 to 450 K

Temperature (K)	Specific volume $\nu_c \times 10^{-3}$ (m^3/kg; P = 0 MPa)				Specific volume $\nu_c \times 10^{-3}$ (m^3/kg; P = 100 MPa)				Specific volume $\nu_c \times 10^{-3}$ (m^3/kg; P = 200 MPa)			
	$\nu_{c\ exp}$ [a]	$\nu_{c\ min}$ [b] (ν_p = 0.30)	$\nu_{c\ avg}$ [b] (ν_p = 0.32)	$\nu_{c\ max}$ [b] (ν_p = 0.44)	$\nu_{c\ exp}$ [a]	$\nu_{c\ min}$ [b] (ν_p = 0.30)	$\nu_{c\ avg}$ [b] (ν_p = 0.32)	$\nu_{c\ max}$ [b] (ν_p = 0.44)	$\nu_{c\ exp}$ [a]	$\nu_{c\ min}$ [b] (ν_p = 0.30	$\nu_{c\ avg}$ [b] (ν_p = 0.32)	$\nu_{c\ max}$ [b] (ν_p = 0.44)
300	0.47	0.47	0.48	0.58	0.46	0.46	0.47	0.57	0.45	0.45	0.46	0.57
350	0.49	0.49	0.50	0.60	0.48	0.48	0.49	0.59	0.46	0.46	0.47	0.59
400	0.50	0.50	0.51	0.61	0.49	0.49	0.50	0.60	0.47	0.48	0.49	0.60
450	0.52	0.52	0.53	0.63	0.50	0.49	0.50	0.60	0.48	0.48	0.49	0.60

[a] measured experimentally

[b] Estimated using Eq. 9

feedstock on a tensile-bar geometry (Fig. 1). Further details about the results from injection-molding experiments are provided elsewhere [23]. Figure 1b shows a 100 % filled tensile bar obtained from an injection-molding experiment. Injection molding simulations were performed for process conditions similar to that of injection-molding experiments using AlN feedstock datasets to understand the effectiveness of PIM simulations in predicting mold-filling behavior. AlN feedstock experimental dataset and dataset 1 from Table 9 were used as inputs for performing simulations. Simulations with the experimental dataset and dataset 1 (Table 9) resulted in 100 % filled part (Fig. 1c, d). The part weight for injection-molding experiments was ~9.95 ± 0.02 g while the part weight was predicted within ±0.5 % for both the datasets. The linear shrinkage for injection-molding experiments was ~0.8 ± 0.15 % while the linear shrinkage predicted within ±0.13 % for both the datasets. The above results indicate the suitability of the Moldflow simulation platform to reasonably capture results from injection-molding experiments. Further, the correspondence in mold-filling predictions between experimentally measured and estimated values of feedstock properties appear to be reasonable for at least simple geometries and warrant further investigation with more complex geometries, such as the heat-sink components evaluated in this paper.

3.3 Application of simulation

The applicability of simulations in practical applications was studied on two types of heat-sink substrate geometries as shown in Fig. 2. A ".udb" catalog file was created for experimental and estimated AlN feedstock properties presented in Tables 2, 3, 4, 6, and 8**.** For the current study, seven datasets of AlN feedstock properties were cataloged and their details are listed in Table 9. To perform simulations for each of the seven datasets, a set of process input parameters were identified. An injection location was selected at the bottom face of the heat-sink substrate since it provides uniform flow distribution of melted feedstock throughout the geometry. Injection-molding simulations were performed for each of the seven datasets presented in Table 9.

The selected input parameters for the current simulation study are represented in Table 10. Injection time was set at 0.1 s, mold and melt temperatures were set at 308 and 423 K while velocity to pressure switchover (V/P) point was selected as 99 %. This set of process input parameters were selected as the injection pressure and volumetric shrinkage results for experimental AlN feedstock dataset lie in the optimum processing range for both heat-sink substrate geometries.

The first set of injection mold simulation comparisons was conducted for the experimental AlN feedstock property dataset and estimated AlN feedstock property datasets 1–3 (Table 9). The process simulation results are divided into flow, temperature, and pressure-related output parameter. Dataset 1

Table 8 Dual-domain Tait constants for AlN feedstock

Dual-domain Tait constants	$\nu_{c\ exp}$ [a]	$\nu_{c\ min}$ [b] (ν_p = 0.30)	$\nu_{c\ avg}$ [b] (ν_p = 0.32)	$\nu_{c\ max}$ [b] (ν_p = 0.44)
b_5 (K)	331	331	331	331
b_6 (K/Pa)	1.30×10^{-7}	1.30×10^{-7}	1.30×10^{-7}	1.30×10^{-7}
b_{1m} (m^3/kg)	4.64×10^{-4}	4.75×10^{-4}	5.77×10^{-4}	4.64×10^{-4}
b_{2m} (m^3/kg K)	1.87×10^{-7}	1.88×10^{-7}	1.95×10^{-7}	1.87×10^{-7}
b_{3m} (Pa)	2.05×10^{9}	1.79×10^{9}	2.17×10^{9}	1.65×10^{9}
b_{4m} (1/K)	4.60×10^{-3}	3.58×10^{-3}	6.15×10^{-3}	2.25×10^{-3}
b_{1s} (m^3/kg)	4.55×10^{-4}	4.67×10^{-4}	5.69×10^{-4}	4.56×10^{-4}
b_{2s} (m^3/kg K)	2.05×10^{-7}	2.05×10^{-7}	2.05×10^{-7}	2.05×10^{-7}
b_{3s} (Pa)	2.52×10^{9}	1.56×10^{9}	1.63×10^{9}	1.31×10^{9}
b_{4s} (1/K)	3.01×10^{-3}	5.88×10^{-3}	6.35×10^{-3}	4.21×10^{-3}
b_7 (m^3/kg)	5.08×10^{-5}	4.73×10^{-5}	5.34×10^{-5}	4.09×10^{-5}
b_8, (1/K)	8.54×10^{-1}	8.62×10^{-1}	8.97×10^{-1}	8.17×10^{-1}
b_9 (1/Pa)	5.06×10^{-6}	5.25×10^{-6}	3.53×10^{-5}	5.19×10^{-6}

[a] Calculated from Eqs. 10 to 13 and experimental (ν_c) values from Table 7

[b] Calculated from Eqs. 1 to 13 and estimated (ν_c) values from Table 7

in Table 9 represents average estimated feedstock properties for AlN. Dataset 2 in Table 9 represents minimum (lowest) estimated feedstock properties for AlN and dataset 3 in Table 9 represents maximum (highest) estimated feedstock properties for AlN. It was observed that flow and temperature-related output parameters of estimated datasets 1–3 had a close match to that of experimental output parameters. Pressure-related output parameters for datasets 1–3 were overestimated when compared with experimental dataset output parameters. As suggested in a previous work by our research group, the cause for such overestimation can be attributed to sensitivity of viscosity estimates towards pressure-related output parameters [2]. To understand the sensitivity of viscosity on pressure-related output parameters, datasets 4–6 were created by substituting estimated feedstock viscosity with experimental feedstock viscosity data (Table 9). The defect evolution was studied by analyzing location of air traps and weld lines both for experimental and estimated datasets.

3.3.1 Flow-related output parameters

The progressive mold-filling behavior observed by using the experimental feedstock property dataset for the heat-sink substrate without fin is shown in Fig. 5a while progressive mold filling for heat-sink substrate with fin is shown in Fig. 5b. A similar progressive mold-filling behavior was observed for simulations using estimated AlN feedstock property datasets 1–3 (Table 9) for both the heat-sink substrate geometries.

Table 9 AlN feedstock datasets used for injection-molding simulations

AlN feedstock dataset	Density[a] (ρ_c, kg/m^3)	Specific heat[b] (C_{pc}, J/kg K)	Thermal conductivity[c] ($\boldsymbol{\lambda_c}$, W/m K)	Cross-WLF constants[d]	Dual-domain Tait constants[e]
Experimental	$\rho_{c\ exp}$	$C_{pc\ exp}$	$\lambda_{c\ exp}$	$\eta_{c\ exp}$	$\nu_{c\ exp}$
1	$\rho_{c\ avg}$	$C_{pc\ avg}$	$\lambda_{c\ avg}$	$\eta_{c\ avg}$	$\nu_{c\ avg}$
2	$\rho_{c\ min}$	$C_{pc\ min}$	$\lambda_{c\ min}$	$\eta_{c\ min}$	$\nu_{c\ min}$
3	$\rho_{c\ max}$	$C_{pc\ max}$	$\lambda_{c\ max}$	$\eta_{c\ max}$	$\nu_{c\ max}$
4	$\rho_{c\ avg}$	$C_{pc\ avg}$	$\lambda_{c\ avg}$	$\eta_{c\ exp}$	$\nu_{c\ avg}$
5	$\rho_{c\ min}$	$C_{pc\ min}$	$\lambda_{c\ min}$	$\eta_{c\ exp}$	$\nu_{c\ min}$
6	$\rho_{c\ max}$	$C_{pc\ max}$	$\lambda_{c\ max}$	$\eta_{c\ exp}$	$\nu_{c\ max}$

[a] Data from Table 2

[b] Data from Table 3

[c] Data from Table 4

[d] Data from Table 6

[e] Data from Table 8

Table 10 Process input parameters for injection-molding simulations

Input parameters	Values
Fill time	0.1 s
Velocity to pressure switch over	99 %
Mold temperature	308 K
Melt temperature	423 K

3.3.2 Temperature-related output parameters

Part weights result comparisons for heat-sink substrate with and without fins are presented in Fig. 6**.** The part weight was determined from the room temperature density value (Table 2) and the total volume defined for the meshed geometry (Fig. 4). It was observed that part weights both for experimental AlN feedstock property dataset (Table 9) and estimated AlN feedstock property datasets 1–3 (Table 9) were higher for the heat-sink substrate with fins. This increase in part weights for heat-sink substrate with fins can be attributed to the increase in part volume due to the addition of fins. Part weights for the experimental dataset and estimated dataset 1 were comparatively similar with an error of 2 % for both the heat-sink substrate geometries. It was observed that part weight increases with a decrease in feedstock property estimates. The maximum feedstock property estimate, dataset 3 (Table 9), has the lowest part weight while the minimum feedstock property estimate dataset 2 (Table 9) has the highest part weight.

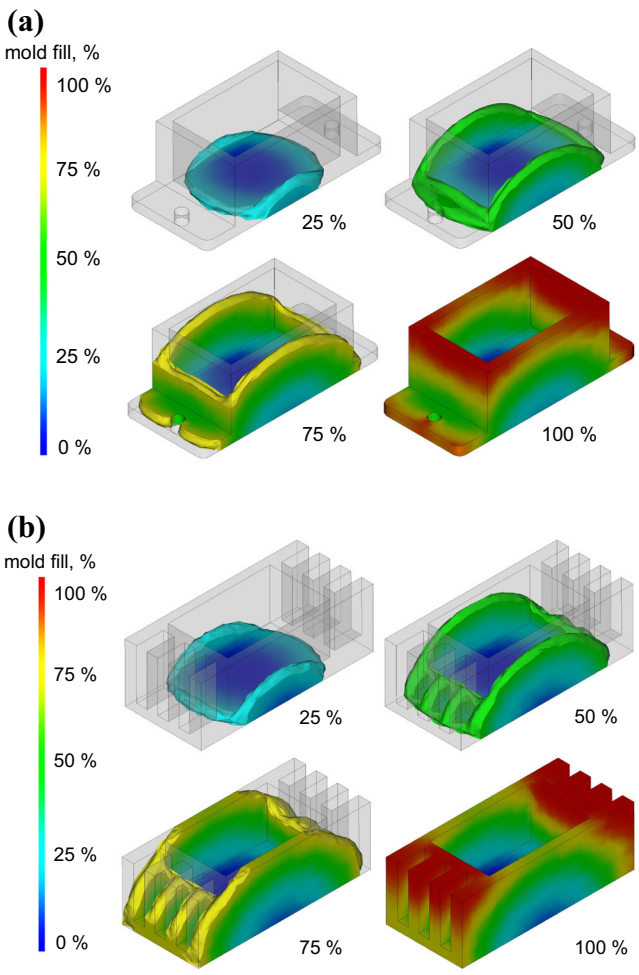

Fig. 5 **(a)**. General progressive mold-filling behavior observed for heat-sink substrate without fins. **(b)**. General progressive mold-filling behavior observed for heat-sink substrate with fins

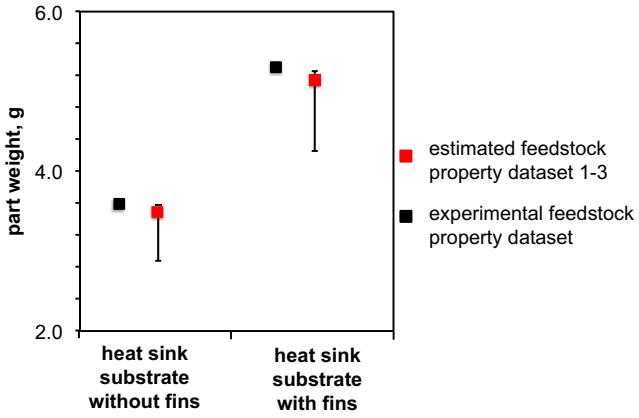

Fig. 6 Comparison of part weight for heat-sink substrates with fins and without fins using the experimental feedstock property dataset and estimated feedstock property datasets 1–3 (Table 9)

Percent volumetric shrinkage result comparisons for the heat-sink substrate without fins and with fins are presented in Fig. 7. The volumetric shrinkage calculations were based on the difference between the PvT state during molding and the reference state where pressure (P) is 0 MPa and temperature (T) is at ambient temperature of 298 K (Fig. 4). For ceramic-filled polymers, the percent volumetric shrinkages have been reported to range between 1.2 and 2.4 % [34]. It can be observed from Fig. 7 that volumetric shrinkage for the experimental AlN feedstock property dataset is ~1.2 % while volumetric shrinkage from the estimated AlN feedstock property datasets 1–3 are in the range of 0.98–1.3 %. The percent volumetric shrinkage for experimental dataset and estimated

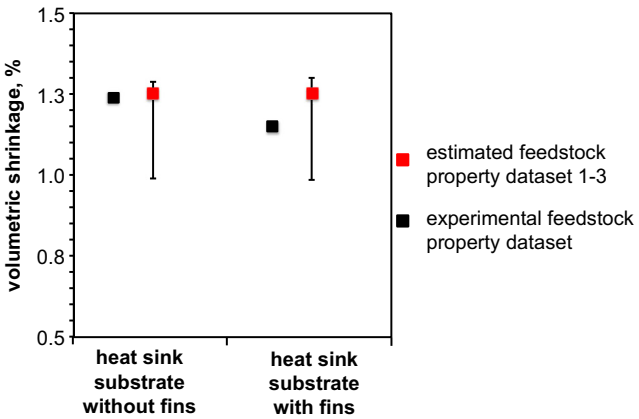

Fig. 7 Comparison of percent volumetric shrinkage for heat-sink substrates with fins and without fins using the experimental feedstock property dataset and estimated feedstock property datasets 1–3 (Table 9)

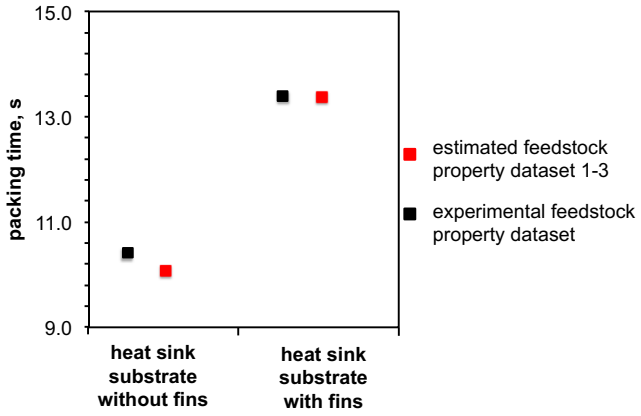

Fig. 8 Comparison of packing time for heat-sink substrates with fins and without fins using the experimental feedstock property dataset and estimated feedstock property datasets 1–3 (Table 9)

dataset 1 are comparatively similar with an error of 0.8 % for the heat-sink geometry without fin and an error of 6 % for the heat-sink substrate with fins. The volumetric shrinkage ranges shown in Fig. 7 for datasets 1–3 correspond to the simulated values using the minimum and maximum feedstock property datasets. The maximum feedstock property estimates, dataset 3 (Table 9), showed the lowest shrinkage (minimum value in Fig. 7) while the minimum feedstock property estimates, dataset 2 (Table 9) showed the highest shrinkage (maximum value in Fig. 7).

Packing times result comparisons for heat-sink substrate without fins and with fins are presented in Fig. 8. Packing time in injection molding starts when the mold is filled completely and ends when the packing pressure is released. In the packing stage, pressure is applied to the feedstock melt to compress the polymer so that more feedstock gets filled into the mold. Packing times are dependent on the heat transfer rate and amount of heat needed to cool the feedstock from melting temperature to ambient temperature. It can be observed from Fig. 8 that packing times for experimental feedstock property dataset (Table 9) and estimated feedstock property datasets 1–3 (Table 9) were comparatively same for both heat-sink substrate geometries. Packing times showed no sensitivity for estimated datasets 1–3 indicating that variation in thermal conductivity and specific heat estimates do not correspond to variations in packing times. If thermal conductivity and specific heat are estimated in same order of magnitude as that of experimental measurements then the corresponding packing time estimates can be predicted reasonably well. Additionally, it was observed that heat-sink substrate with fins have higher packing times due to their higher volumes.

3.3.3 Pressure-related output parameters

Injection pressure comparisons for both the heat-sink substrate geometries are presented in Fig. 9**.** Injection pressure is the pressure applied to the feedstock melt by the ram during the

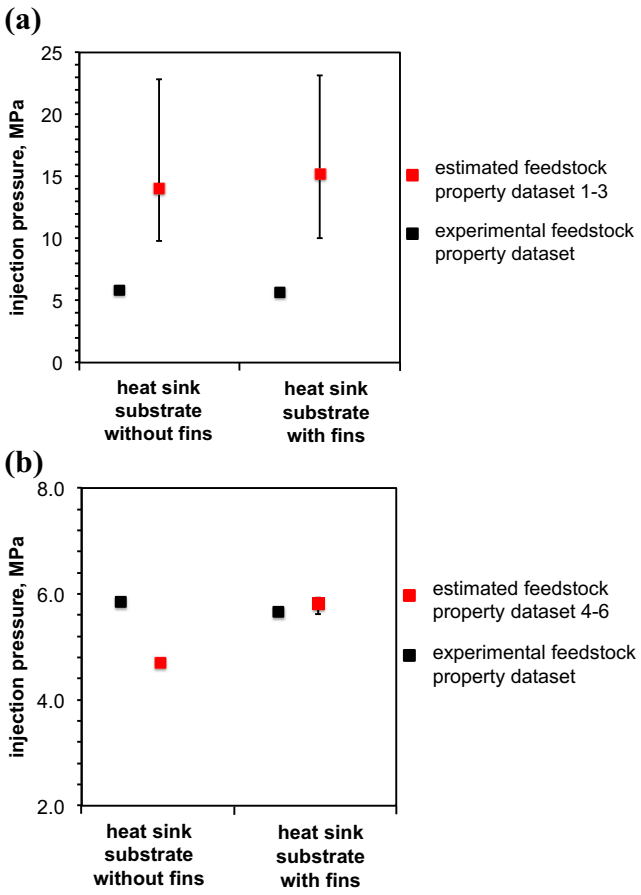

Fig. 9 **a**.) Comparison of injection pressure for heat-sink substrates with fins and without fins using the experimental feedstock property dataset and estimated feedstock property datasets 1–3 (Table 9).**b**.) Comparison of injection pressure for heat-sink substrates with fins and without fins geometry using the experimental feedstock property dataset and estimated feedstock property datasets 4–6 (Table 9)

mold-filling stage that causes the material to flow inside the cavity and later during packing stage to compress the feedstock melt inside the cavity. The maximum pressure at the nozzle during the filling phase when the switch over occurs from velocity filled to pressure filled (Table 10) is referred to as the injection pressure in simulations. Large pressure gradients during mold-filling stage are a sign of flow imbalance due to improper gate location and very small or very high fill times [35]. Therefore, identifying minimum injection pressures that provide the least amount of shrinkage are best for obtaining a quality part with no defects. It can be observed in Fig. 9a that injection pressures for estimated feedstock property datasets 1–3 are higher by a factor of 10 when compared with injection pressures obtained from experimental feedstock property dataset (Table 9) for both heat-sink substrate geometries.

To account for the overestimation in injection pressure, the viscosity estimates were substituted with experimental values from viscosity measurements and datasets 4–6 were created [2]. It can be observed from Fig. 9b that the injection pressures for datasets 4–6 were comparatively close to the injection

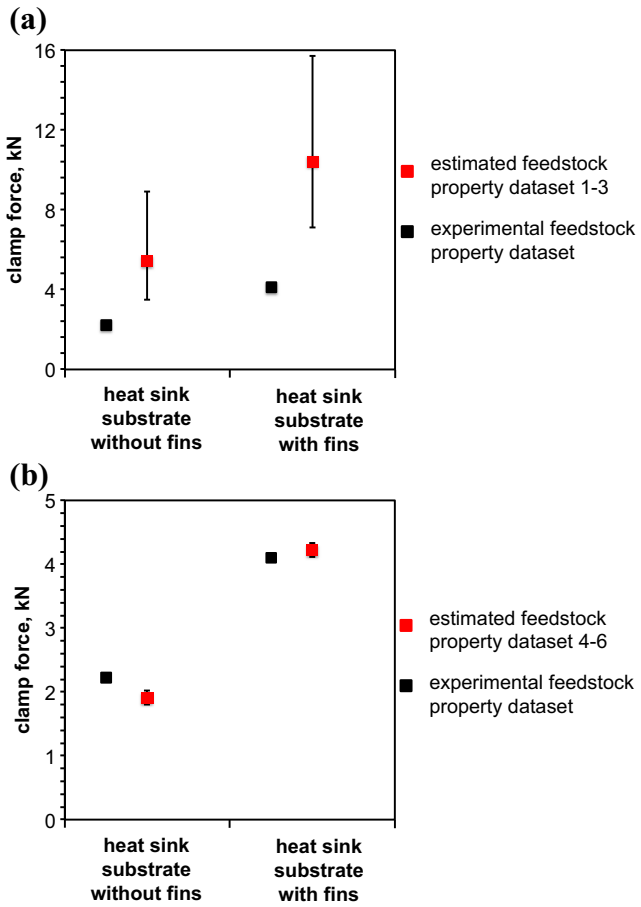

Fig. 10 **a)** Comparison of clamp force for heat-sink substrates with fins and without fins using the experimental feedstock property dataset and estimated feedstock property satasets 1–3 (Table 9). **b)** Comparison of clamp force for heat-sink substrates with fins and without fins using the experimental feedstock property dataset and estimated feedstock property datasets 4–6 (Table 9)

pressure obtained from using the experimental feedstock dataset (Table 9). Therefore, an improvement in viscosity estimates is necessary to obtain accurate injection pressure estimates and is a part of our future study.

The clamp force is another pressure-related output parameter. It is the maximum force required to keep the mold closed during the filling stage. Clamp force is a function of injection pressure and the area of the part projected onto the XY plane. It can be observed in Fig. 10a that the clamp force for estimated feedstock property datasets 1–3 were slightly higher when compared with clamp force obtained from experimental feedstock property dataset (Table 9) for both the heat-sink substrate geometries.

To account for the overestimation in clamp force, the viscosity estimates were substituted with experimental values from viscosity measurements and datasets 4–6 were created due to sensitivity of clamp force towards viscosity [2]. It can be observed from Fig. 10b that clamp force for datasets 4–6 were comparatively close to the clamp force obtained by using the experimental feedstock dataset (Table 9). A further improvement in viscosity estimates is therefore necessary in order to obtain accurate clamp force estimates and is a part of our future study.

4 Conclusions

The present study indicates the merit of using estimated feedstock properties as input parameters in mold-filling simulations that could be extended for a variety of material systems and geometries early in the PIM design stage. The approach developed in the present study provides the following key conclusions:

1. Literature filler properties used in conjunction with mixture models for predicting the physical, thermal, and rheological properties of AlN feedstocks provide comparable (within the same order of magnitude) estimates to experimentally measured feedstock properties for AlN.
2. Mold-filling simulations performed using estimated and experimentally measured AlN feedstock properties show reasonable correspondence to injection-molding experiments for a simple tensile-bar geometry.
3. Mold-filling simulations performed for more complicated heat-sink geometries clearly indicate that similar results could be obtained by using estimated and experimentally measured AlN feedstock properties (datasets 1–3) for predicting mold-filling behavior, part weight, % volumetric shrinkage, and packing time but were underestimated for clamp force and injection pressure.
4. Using a combination of estimated AlN feedstock properties and experimentally measured viscosity (datasets 4–6) improved the correspondence to simulation results that solely used experimentally measured AlN feedstock properties for injection pressure and clamp force predictions of complex heat-sink geometries. This result indicates that improved methodologies for estimating shear rate and temperature-dependent viscosity of highly filled polymers are needed in the future to continue to build on the advantages provided by the present work.

Acknowledgment The authors thank the financial support obtained from the National Science Foundation (CMMI 1200144).

References

1. German RM, Atre SV (2013) PIM 2013 market study. New York
2. Atre SV, Park S-J, Zauner R, German RM (2007) Process simulation of powder injection moulding: identification of significant parameters during mould filling phase. Powder Metall 50:76–85. doi:10.1179/174329007X185607

3. Urval R, Lee S, Atre SV et al (2008) Optimisation of process conditions in powder injection moulding of microsystem components using a robust design method: part I. primary design parameters. Powder Metall 51:133–142. doi:10.1179/174329008X284796
4. Kate KH, Onbattuvelli VP, Enneti RK et al (2012) Measurements of powder–polymer mixture properties and their use in powder injection molding simulations for aluminum nitride. JOM 64:1048–1058. doi:10.1007/s11837-012-0404-3
5. Ahn S, Chung ST, Atre SV et al (2008) Integrated filling, packing and cooling CAE analysis of powder injection moulding parts. Powder Metall 51:318–326. doi:10.1179/174329008X284903
6. Park S-J, Ahn S, Kang TG et al (2010) A review on computer simulations in powder injection molding. Int J Powder Metall 46:37–46
7. Onbattuvelli VP, Enneti RK, Park S-J, Atre SV (2013) The effects of nanoparticle addition on SiC and AlN powder–polymer mixtures: packing and flow behavior. Int J Refract Met Hard Mater 36:183–190. doi:10.1016/j.ijrmhm.2012.08.014
8. Onbattuvelli VP (2010) The effects of nanoparticle addition on the processing, structure and properties of SiC and AlN
9. Groza JR, Zavaliangos A (2000) Sintering activation by external electrical field. Mater Sci Eng A 287:171–177. doi:10.1016/S0921-5093(00)00771-1
10. Biswas K, Schneider J, Rixecker G, Aldinger F (2005) Comparative bending creep behaviour of silicon carbide sintered with oxynitride additives. Scr Mater 53:591–596. doi:10.1016/j.scriptamat.2005.04.024
11. Gu J, Zhang Q, Dang J et al (2009) Thermal conductivity and mechanical properties of aluminum nitride filled linear low-density polyethylene composites. Polym Eng Sci 49:1030–1034. doi:10.1002/pen.21336
12. Kochetov R, Andritsch T, Lafont U et al (2009) Preparation and dielectric properties of epoxy - BN and epoxy - AlN nanocomposites. In: IEEE Electr Insul Conf 2009 EIC 2009 pp 397–400
13. Zhou W (2011) Thermal and dielectric properties of the AlN particles reinforced linear low-density polyethylene composites. Thermochim Acta 512:183–188. doi:10.1016/j.tca.2010.10.003
14. Zhu BL, Ma J, Wu J et al (2010) Study on the properties of the epoxy-matrix composites filled with thermally conductive AlN and BN ceramic particles. J Appl Polym Sci 118:2754–2764. doi:10.1002/app.32673
15. Risbud SH, Groza JR, Kim MJ (1994) Clean grain boundaries in aluminium nitride ceramics densified without additives by a plasma-activated sintering process. Philos Mag Part B 69:525–533. doi:10.1080/01418639408240126
16. Khor KA, Cheng KH, Yu LG, Boey F (2003) Thermal conductivity and dielectric constant of spark plasma sintered aluminum nitride. Mater Sci Eng A 347:300–305. doi:10.1016/S0921-5093(02)00601-9
17. Medraj M Understanding AlN sintering through computational thermodynamics combined with experimental investigation. J Mater Process Tech 161:415–422
18. Qiao L, Zhou H, Fu R (2003) Thermal conductivity of AlN ceramics sintered with CaF2 and YF3. Ceram Int 29:893–896. doi:10.1016/S0272-8842(03)00033-6
19. Miyashiro F, Iwase N, Tsuge A et al (1990) High thermal conductivity aluminum nitride ceramic substrates and packages. IEEE Trans Compon Hybrids Manuf Technol 13:313–319. doi:10.1109/33.56163
20. Cardarelli F (2008) Materials handbook: a concise desktop reference. Springer Science & Business Media
21. Bae J-W, Kim W, Cho S-H, Lee S-H (2000) The properties of AlN-filled epoxy molding compounds by the effects of filler size distribution. J Mater Sci 35:5907–5913. doi:10.1023/A:1026741300020
22. Bauccio M (1994) ASM engineered materials reference book. ASM International
23. Granta's CES EduPack and teaching resources: supporting Materials Education. http://www.grantadesign.com/education/. Accessed 27 Sep 2013
24. Jackson TB, Virkar AV, More KL et al (1997) High-thermal-conductivity aluminum nitride ceramics: the effect of thermodynamic, kinetic, and microstructural factors. J Am Ceram Soc 80:1421–1435. doi:10.1111/j.1151-2916.1997.tb03000.x
25. Slack GA (1964) Thermal conductivity of pure and impure silicon, silicon carbide, and diamond. J Appl Phys 35:3460. doi:10.1063/1.1713251
26. YimWM, Paff RJ (1974) Thermal expansion of AlN, sapphire, and silicon. J Appl Phys 45:1456. doi:10.1063/1.1663432
27. Qiao L, Zhou H, Xue H, Wang S (2003) Effect of Y2O3 on low temperature sintering and thermal conductivity of AlN ceramics. J Eur Ceram Soc 23:61–67. doi:10.1016/S0955-2219(02)00079-1
28. Qiao L, Zhou H, Chen K, Fu R (2003) Effects of Li2O on the low temperature sintering and thermal conductivity of AlN ceramics. J Eur Ceram Soc 23:1517–1524. doi:10.1016/S0955-2219(02)00344-8
29. Kate KH, Enneti RK, Park S-J et al (2014) Predicting powderpolymer mixture properties for PIM design. Crit Rev Solid State Mater Sci 39:197–214. doi:10.1080/10408436.2013.808986
30. Ashby MF (2010) Materials selection in mechanical design. Butterworth-Heinemann
31. HaynesWM(2014) CRC handbook of chemistry and physics, 95th edition. CRC Press
32. Center PUTPR (1970) Thermophysical properties ofmatter: specific heat: metallic elements and alloys, by Y. S. Touloukian and E. H. Buyco. IFI/Plenum
33. Nakano H, Watari K, Hayashi H, Urabe K (2002) Microstructural characterization of high-thermal-conductivity aluminum nitride ceramic. J Am Ceram Soc 85:3093–3095. doi:10.1111/j.1151-2916.2002.tb00587.x
34. Smothers WJ (2009) 1981 New England section topical meeting on nonoxide ceramics: ceramic engineering and science proceedings, volume 3, number 1/2. John Wiley & Sons
35. Shoemaker J (2006) Moldflow design guide: 'a resource for plastics engineers. Hanser Publications, Munich